1.11 AIRBORNE MEASUREMENTS IN THE EARLY-MORNING SHALLOW CONVECTIVE BOUNDARY LAYER

Jens Bange and Thomas Spieß

Institute for Aerospace Systems, Technical University Braunschweig, Germany

1. INTRODUCTION

Over land surfaces shortly after sunrise a shallow convective boundary layer (SCBL) develops below the formerly ground-based nocturnal inversion layer (NIL). On a summer morning with low soil water content and a cloudless sky, the top of the SCBL increases rapidly due to heating of the surface, the resulting upward turbulent sensible heat flux H and the entrainment of air from above. This kind of morning transition - the rapid burning off of the nocturnal inversion (Stull 1988) - does possibly not provide enough time for a thorough mixing of the SCBL and the reaching of an equilibrium as observed during the daytime convective boundary layer (CBL).

The early morning transition gives a good opportunity to study CBL characteristics and entrainment. The relevant vertical and horizontal scales are small and allow measurements of the turbulent and convective flow with small statistical uncertainties (Lenschow and Stankov 1986). Furthermore, disturbing effects or complex boundary conditions like clouds do normally not occur. The early morning SCBL is the clear-convective case where strong up- and down-drafts are much more important than subsidence and radiative cooling which can lead to sharp-edged temperature profiles without an interfacial layer. During the morning transition a pronounced entrainment zone can therefore always be expected as long as the synoptical wind speed is low. The general process of the transition is well known. But especially scales and practical values that can be used for numerical models and analytic methods to describe the transition - which has a great relevance to air pollution - are missing.

Corresponding author:
Jens Bange
Institute of Aerospace Systems
Technical University of Braunschweig, Germany
j.bange@tu-bs.de

Past experiments revealed that the morning transition can partly be described by linear and quasi-stationary processes. E.g. the surface heat flux increases linearly in time (Tennekes 1973; Angevine *et al.* 2001) and so does the surface temperature. This raised the question whether the usual Deardorff scaling scheme for the daytime CBL is also applicable although the SCBL is possibly not well mixed. We applied airborne measurements to determine the systematic (and then possibly scalable) behaviour of the flow between the lower part and the top of the SCBL. To cover this height range a somewhat unusual flight strategy at constant altitude was applied.

2. EXPERIMENTAL SETUP

The airborne measurements were performed using the helicopter-borne turbulence probe Helipod (Muschinski and Wode 1998; Bange and Roth 1999; Bange *et al.* 2002). The Helipod (Figure 1) is a unique turbulence measurement system of about 5 m in length, 0.5 m in diameter, and 250 kg in weight. The autonomously operating sensor package was constructed to be carried by almost any helicopter attached to a rope of 15 m length. At a typical ground speed of 40 m s^{-1} the Helipod is outside the downwash area of the rotor blades. Due to its small fuselage, and the absence of wings and propulsion the influence of the Helipod on the atmosphere is small compared to conventional research aircraft. Additionally, the Helipod is in general allowed to perform lower and slower flights than an air plane.

The Helipod carries its own navigation systems, power supply, data storage and fast responding sensor equipment. The system was designed for *in situ* measurements of the turbulent fluctuations of wind, temperature, humidity and the turbulent fluxes. To achieve a high temporal resolution, each meteorological parameter was measured with at least two different types of instruments: One that had a short response time, but

Fig. 1: The turbulence probe Helipod during take off at the research airport Braunschweig.

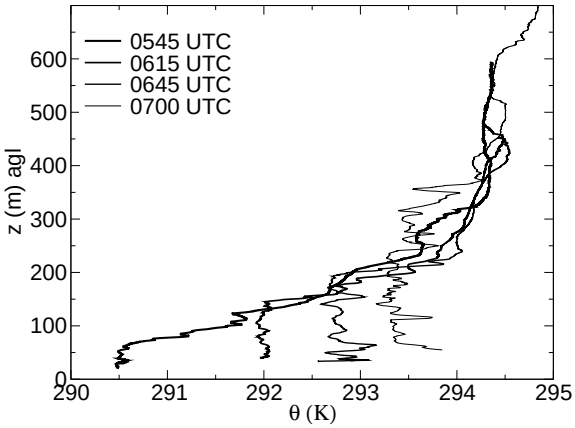

Fig. 2: Four vertical profiles of the potential temperature θ successively measured by the Helipod on 8 July, 2002. The data were smoothed by a moving average over 8 s.

the disadvantage of a temporal drift, was sampled at 100 Hz. The other type responded slowly but was very accurate on a large time scale, and was sampled at 20 Hz. To achieve a large frequency range the data sets were combined by complementary filters. The results were 100 Hz time series of the meteorological parameters, equivalent to one measurement point every 40 cm. To achieve an even higher resolution the Helipod was upgraded in 2005 to 500 Hz sampling rate and CO_2 measurement. The system can optionally be equipped with additional sensors e.g. aerosol probes.

The Helipod performed 40 hours of measurement flights during the STINHO-2 (**ST**ructure of the turbulent transport over **INHO**mogeneous surfaces) experiment in 2002 (Raabe *et al.* 2005) which was embedded into the series of the LITFASS experiments (Beyrich *et al.* 2002c; Neisser *et al.* 2002). The experimental site was located near the meteorological observatory Lindenberg (MOL) of the German meteorological service (DWD) about 60 km south-east of Berlin. Among others, seven micro-meteorological stations were installed on different surface types as well as a large aperture scintillometer (LAS, Beyrich *et al.* 2002b) and a 99 m meteorological tower (Beyrich *et al.* 2002a).

On three days the early-morning boundary-layer transition was probed (Table 1). In general the nights before the flights were cloudless with the exception of a few cirrus clouds. The resulting strong nocturnal net radiative cooling caused a ground-based inversion with a vertical potential temperature gradient of $\gamma_i = \partial\theta\ (\partial z)^{-1}$ =1.3...2 K (100 m)$^{-1}$. The vertical temperature profile within the inversion was non-uniform and exhibited many thin layers with various lapse rates, as typical for a stably stratified flow (Gossard *et al.* 1985). The top of the inversion was found between h = 240 and 390 m with some dependence on the location of the vertical sounding. Above h the atmosphere (the residual layer RL) was slightly stably or neutrally stratified. At the bottom of the RL wind speeds around 5 m s^{-1} were observed. Convection reached the flight level between 05 and 06 UTC (local time was UTC plus two hours). The NIL was completely removed about one hour later (Figure 2). Before that, the NIL acted like a lid on the developing SCBL,

similar to the daytime capping inversion. During the burning off the mean lapse rate γ_i inside the inversion was not changing.

The Helipod performed so-called 'Small Grid' low-level flight patterns which consisted of 13 to 15 straight and level legs of 5 km length, half of them oriented in north-south and half of them in west-east direction (Figure 3). The centre of the flight pattern was the 99 m tower of the German Meteorological Service DWD at Falkenberg. The transmitter of the LAS was mounted on the 99 m tower at Falkenberg, while the receiver was mounted on a platform at the MOL site, 4.7 km northward (Beyrich *et al.* 2002b).

The horizontal flights at about $z = 80$ m agl were supplemented by slant flights at the corners of the square-shaped flight pattern. These vertical soundings reached up to 800 m agl. Detailed information on the analysed flights is given in Table 1.

In the daytime CBL vertical profiles of statistical moments like the line-averaged turbulent fluxes are usually obtained from measurement flights at various levels with respect to the ground. The rapid development of the SCBL during the morning transition gave an opportunity for a different flight strategy: While the Helipod stayed at a constant height z, the top of the SCBL was rising rapidly. On one hand the flight legs were long enough to provide reasonable statistical errors of the turbulent fluxes in stable stratification. On the other hand the time to fly the legs was short enough (two minutes) to be interpreted as a snap-shot of the turbulent flow. Goal of the strategy was to weight the flight level z with a certain scaling height z_i (e.g. the current depth of the SCBL) to obtain vertical flux profiles in terms of a dimensionless height ζ.

3. CHARACTERISTICS OF THE SCBL

In the daytime, well-mixed CBL large-scale convective motion driven by surface heating force a near-uniform distribution of the mean wind vector $\langle \vec{v} \rangle$ and the potential temperature θ. The controlling parameters are the scaling height z_i of the CBL and the surface heat flux

$$H_0 = \rho c_p \left\langle w' \theta' \right\rangle |_{z=0} \qquad (1)$$

with air density ρ, specific heat c_p and vertical wind fluctuations w'. The brackets denote averaging and the prime indicates fluctuations i.e., quantities subtracted by their mean value and by their linear trend. In the following the scaling parameters and other quantities are derived accordingly to the daytime well-mixed CBL.

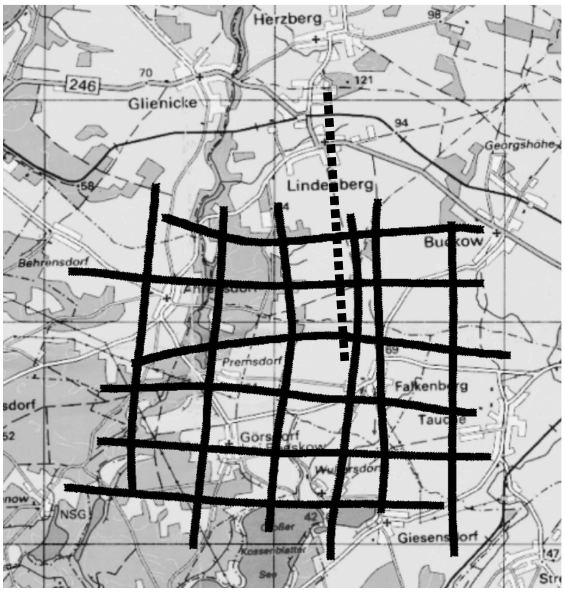

Fig. 3: 'Small Grid' flight pattern of the Helipod and measurement path of the LAS (dotted line).

3.1 Scaling Heights

A CBL can generally be described by three characteristic heights (e.g. Sorbjan 1995):

- The top h of the entire boundary layer which is identical with the bottom of the free atmosphere in the day time CBL. During the morning transition h can be identified with the base of the RL of the CBL of the afternoon before. Above h the morning ABL is neutrally or slightly stably stratified. During the flight experiment h was found to be stationary on a horizontal average (Table 1).
- The base h_i of the thermal inversion. Above h_i the potential temperature θ is increasing. Below h_i the ABL flow is turbulent and convective. The base itself is rising in time due to the burning-off process.
- The buoyancy flux zero-crossing height h_0

marks the altitude where the sensible heat flux becomes negative the first time.

The height h_0 is located clearly below the inversion at h_i (e.g., Sorbjan 1995). Both heights can be set into a linear relationship which is possibly valid for a certain time period:

$$\frac{h_0}{h_i} =: B \tag{2}$$

where B is positive and always smaller than unity. For the daytime CBL the normalised zero-crossing height B is a function of the entrainment parameter A (Sorbjan 1995)

$$A \;=\; -\frac{H_i}{H_0} \;=\; \frac{1}{B} - 1 \;, \tag{3}$$

with the minimum heat flux $H_i < 0$ of the ABL and the surface heat flux H_0. A typical value of the daytime entrainment parameter is $A \approx 0.2$ (Sorbjan 1996b; Kim *et al.* 2003), leading to a rough estimate of $h_0 \approx 0.83\ h_i$ in the well-mixed CBL. Results from LES showed that this is a slight over-estimation and rather suggest $B \approx 0.75$ (Sorbjan 1995).

The top of the mixing layer z_i was determined by eye from the slant profiles performed by the Helipod in between horizontal legs (Figure 2) and compared to sodar and tower observations (Figure 4). All measurements displayed a steady and uniform rise of the inversion base so that the temporal increase of the scaling height could be described by

$$\dot{z}_i \;\equiv\; \frac{\partial z_i}{\partial t} \;\approx\; \text{constant} \,. \tag{4}$$

Considering that a) the sodar data were not available for all investigated days, b) the mixing height estimation from sodar data is not always reliable especially in complex terrain (Beyrich 1997), and c) the tower data seemed to fit better with the Helipod data, only the latter was used for the further analysis. For all three morning transitions the expansion speed $\dot{z}_i$ of the SCBL was about 140 m per hour (Table 1).

As a result of the rapidly increasing inversion height, each leg of the grid flight patterns had to be assigned to a different value of the dimensionless height $\zeta \;=\; z\ {z_i}^{-1}$. The values of ζ for each individual leg were calculated by linear interpolation of z_i as observed during the Helipod slant

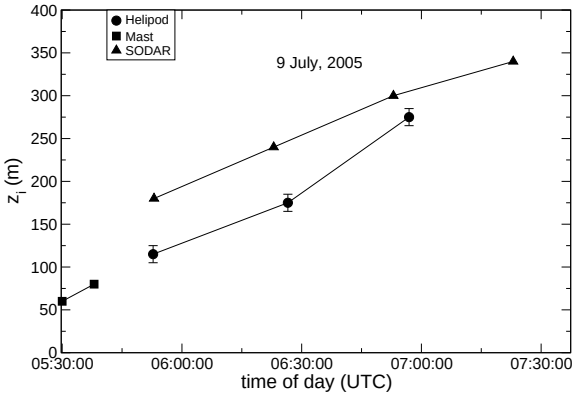

Fig. 4: Time series of inversion height z_i determined from tower and sodar measurements and steep-slant Helipod flights on 9 July.

profiles (Figure 4). Thus the early legs were performed just below $\zeta = 1$, while the latest legs were located at $\zeta \approx 0.25$. About then the SCBL reached the top of the inversion h and the convective elements ascended without the cushioning effect of an topping inversion into the RL.

3.2 Surface Heat Flux

The current surface flux for each individual leg was sought for proper scaling. In principle, the surface heat flux H_0 can be determined from single-altitude low-level flights in combination with an inverse model (LLF+IM method, see Bange *et al.* 2006). The method relies on a low horizontal flight that spans at least a square-shaped pattern so that the numerical inversion is able to distinguish temporal and spatial dependence. Since the single legs of the Small Grid flight pattern did not provide information on the horizontal distributions, the LLF+IM method could not be applied here. Instead of that the surface heat flux had to be determined from simultaneous ground-based measurements that covered an area large enough to be representative for the $5 \times 5\ \mathrm{km}^2$ investigation site.

During STINHO-2 the synoptic wind speed was low and the early morning SCBL was not well horizontally mixed. Therefore, the measurements of the 99 m tower were not representative for the investigated area and were not taken into account. The LAS was the most suitable measurement system for the comparison with the Heli-

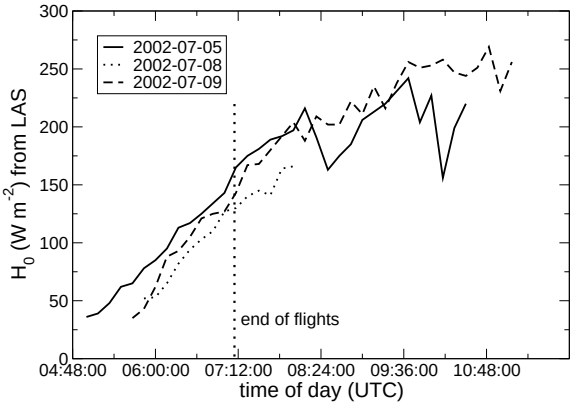

Fig. 5: Time series of sensible surface heat flux measured by LAS (10-minutes averages). The dotted line indicates the end of the early morning flight measurements.

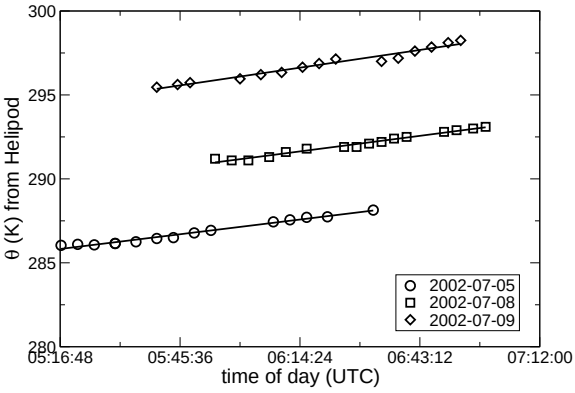

Fig. 6: Time series of potential temperature measured at constant altitude by the Helipod.

pod because it also measured over a mixture of surface types (forest, grassland, grain crop fields, rape fields etc.) with a path length of 4.7 km (Figure 3). The method to calculate surface fluxes from LAS over heterogeneous terrain was described in detail by Meijninger *et al.* (2002) and Meijninger *et al.* (2005). The relative error of the surface heat flux H_0 derived from the LAS was estimated as about 10-15 %. This uncertainty was basically due to some simplifying assumptions when deriving H_0 from the measurements of the refractive index structure parameter and to the possible range of the similarity coefficients used thereby. The flux data were determined as ten-minute averages (Figure 5). During the measurement flights (until 07 UTC) the increase of the surface flux was well approximated by a linear process i.e.

$$\dot{H}_0 \equiv \frac{\partial H_0}{\partial t} \approx \text{constant} \tag{5}$$

as already reported by Tennekes (1973). During the three early-morning flights in STINHO-2, $\dot{H}_0 \approx 60$ W m^{-2} h^{-1} was observed (Table 1).

3.3 Thermal Structure of the SCBL

The thermal budget of a CBL can be described by (e.g., Betts *et al.* 1990)

$$\frac{1}{\rho c_p}\frac{\partial H}{\partial z} = -\frac{\partial \theta}{\partial t} - S \tag{6}$$

where S denotes the horizontal turbulent fluxes and the advection due to the mean wind vector $\langle\vec{v}\rangle = (\bar{u},\bar{v},\bar{w})$

$$S = \langle\vec{v}\rangle \,\mathrm{grad}\,\bar{\theta} + \frac{\partial \overline{u'\theta'}}{\partial x} + \frac{\partial \overline{v'\theta'}}{\partial y}\,. \tag{7}$$

Assuming that the advection S is comparatively small (e.g. Fedorovich *et al.* 2004) the heat flux at height z can be approximated by

$$H(z,t) = \rho c_p \int_z^{h_0} dz' \, \frac{\partial \theta(z',t)}{\partial t} \tag{8}$$

as demonstrated by Sorbjan (1995). In a quasi-stationary situation i.e., with a height independent and constant heating rate $\dot{\theta} \equiv \partial\theta\,(\partial t)^{-1}$, the integration results in

$$H(z) = \rho c_p\,(h_0 - z)\;\dot{\theta} \tag{9}$$

i.e., the vertical heat flux up to h_0 is expected to show a linear height dependence, as usually found in the daytime CBL. Quasi-stationarity could also be assumed during the morning transition (Sorbjan 2005). The potential temperature θ and also the adiabatic lapse rate $\partial\theta(\partial z)^{-1} \approx 0$ were height-independent within the SCBL, although strong fluctuations due to convective elements and turbulence occurred (Figure 2). The potential temperature increased at a constant rate of about 2 K per hour as measured by the Helipod (Figure 6 and Table 1).

Since the buoyancy flux zero-crossing height could not directly be observed, h_0 was substituted using (2). During the burning off the inversion

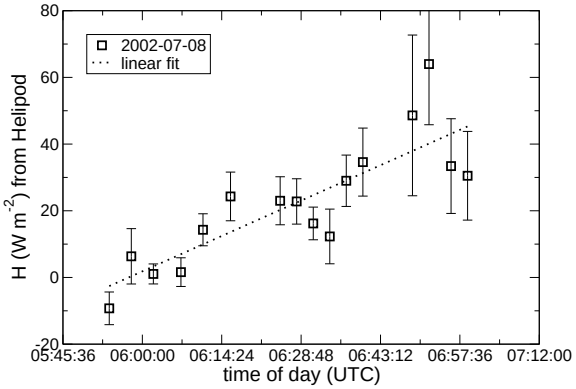

Fig. 7: Time series of sensible heat flux measured by Helipod at constant height of 90 m on 8 July.

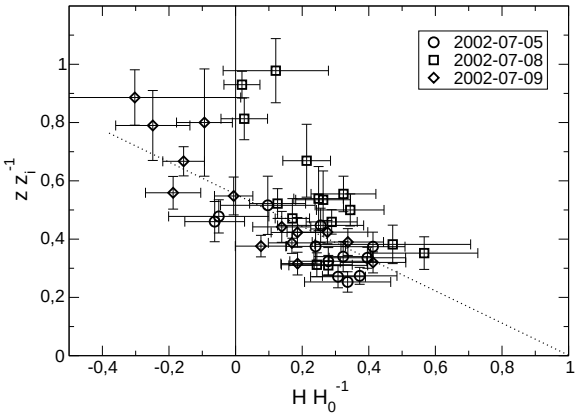

Fig. 8: An attempt of Deardorff-scaling all heat fluxes measured during the three days. The dotted line was drawn by eye.

base z_i was rising. It was assumed that h_0 was also increasing in time. So the ratio B was considered to be approximately constant during the transition. The temporal increase of the heat flux at a fixed altitude z could then be expressed in terms of the scaling inversion height z_i:

$$\dot{H} \equiv \frac{\partial H}{\partial t} = \rho c_p B \dot{\theta} \dot{z}_i . \qquad (10)$$

As a consequence $\dot{H}$ should also be constant and the vertical flux profile was expected to be linear in the Deardorff scaling scheme.

Actually the time series of the heat flux $H(z)$ measured by the Helipod at constant altitude z were not that steady as expected. For instance, Figure 7 shows larger deviation of the measured flux from the linear regression, probably due to the heterogeneous surface of the overflown terrain. Error bars, calculated according to Lenschow and Stankov (1986) with modifications introduced by Bange *et al.* (2006), increased with time due to the increase of the size of the convective elements and corresponding increase of the turbulent integral length scale. The linear regression provided a height ratio $B \approx 0.4$ (Table 1). Thus the heat flux was expected to cross zero shortly below the centre of the SCBL. For comparison, typical values in the daytime CBL are about $h_0 \approx 0.8\, z_i$.

Considering the temporal development of the SCBL, both the height z and the sensible heat flux $H(z)$ were scaled using the Deardorff scheme (Deardorff 1970). Due to the low flight levels the decrease of the air density with height was neglected:

$$\frac{\langle w'\theta' \rangle_z}{\langle w'\theta' \rangle_0} \approx \frac{H(z)}{H_0} . \qquad (11)$$

As expected from the non-linear behaviour of the heat flux time series, the dimensionless heat flux in Figure 8 did not reveal a clear linear dependence on the dimensionless height ζ nor did the data points drop to a joint curve. However, the latter can even not be expected for the daytime CBL, as the variety of entrainment parameters A found in literature demonstrates (see Equation 3). Also the vertical distribution of the dimensionless heat fluxes in the daytime CBL determined in various field experiments (e.g. as collected by Sorbjan 1991) revealed similarly strong scatter. Nevertheless, a linear fit to the data points fulfilled an important criteria: the fit ended at $H(0) = H_0$ i.e., the extrapolated airborne flux measurements were in agreement with the ground-based LAS observations. By the way this was not fulfilled in airborne measurements during the morning hours analysed by de Arellano *et al.* (2004).

The same fitted line crossed zero at 0.55 z_i in acceptable agreement with the expectations for B from the linearised enthalpy equation (6). Unfortunately there were only few data points above h_0 so the interesting region at the top of the SCBL was poorly resolved. But still visible was a further decrease of $H(\zeta)$ until a minimum at about 0.8 to 0.9 z_i was reached, which disagreed with the expectation that the flux minimum was reached at

z_i (Deardorff 1974). Then the flux increased and crossed zero again, as expected.

The height ratio B was considered to be more or less constant during the morning transition. Nevertheless B was not suited for the determination of the entrainment parameter – i.e. (3) was considered not to be valid in the SCBL – since A was decreasing rapidly. The entrainment velocity is defined by (e.g. in zero-order-jump models, Tennekes 1973)

$$w_e \;=\; \dot{z}_i - \overline{w} \;=\; -\frac{\langle w'\theta'_e\rangle}{\Delta\theta} \qquad (12)$$

with the large-scale subsidence $\overline{w}$ and the potential temperature increase (jump) $\Delta\theta$ above the inversion at z_i. Since the morning SCBL is developing rapidly, $\overline{w} \ll \dot{z}_i$ can be assumed. The entrainment parameter can then be written as

$$\frac{\dot{z}_i\,\Delta\theta}{\langle w'\theta'\rangle_0} \;\approx\; \frac{\langle w'\theta'\rangle_e}{\langle w'\theta'\rangle_0} \;\approx\; -A\,. \qquad (13)$$

During the morning transition, the surface heat flux was rapidly increasing while the temperature difference $\Delta\theta$ between SCBL and RL was rapidly reduced. Thus A was rapidly decreasing in time. The minimum heat flux in Figure 8 was around -0.3 H_0 leading to $A = 0.3$ which merely represents an entrainment parameter averaged over all measurements on all three days.

3.4 Scales of the SCBL

Typical scales of the convective mixed layer (Deardorff 1970) are the convective velocity

$$w_* = \left[\frac{g}{\theta}\, z_i\, \langle w'\theta'\rangle_0\right]^{1/3} \qquad (14)$$

and the convective temperature

$$\theta_* = \frac{\langle w'\theta'\rangle_0}{w_*}\,. \qquad (15)$$

Typical values for the convective time scale or large-eddy overturning time (e.g., Sullivan *et al.* 1998)

$$\tau_* = \frac{z_i}{w_*} \qquad (16)$$

are around 600 s for the daytime CBL (e.g. the Wangara data, Hibberd 1996), while for the early morning $\tau_* \approx 1000$ s was expected (Sorbjan 2005). The Helipod measurements in STINHO-2 yield much smaller values (Figure 9), between

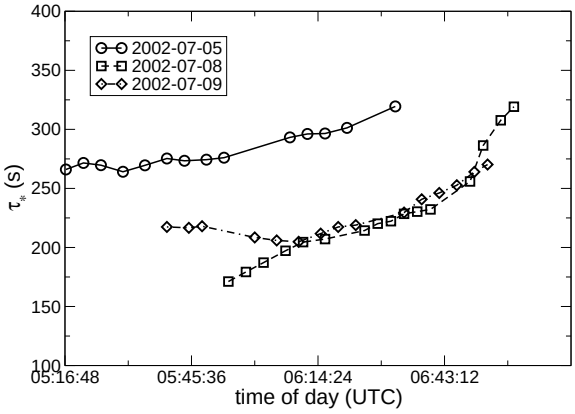

Fig. 9: Time series of the eddy-overturning time τ_* derived from interpolated time series of the inversion height z_i (Helipod) and surface heat flux measurements (LAS), on three different days.

150 and 320 s, slowly increasing with time. This even exceeds observations in strong shear and large vertical wind speeds (Petre and Verlinde 2004). The external forcing time scale

$$\tau_{\rm ext} \;=\; \langle w'\theta'\rangle_0 \left(\frac{\partial\,\langle w'\theta'\rangle_0}{\partial t}\right)^{-1} \;=\; \frac{H_0}{\dot{H}_0} \qquad (17)$$

was at least 1 h (Table 1 and Figure 5). Since $\tau_* \ll \tau_{\rm ext}$, this was another indication for quasi-stationarity during the morning transition.

In the daytime CBL the statistical properties, non-dimensionalised by w_* and θ_*, are expected to be functions only of ζ (e.g., Kaimal and Finnigan 1994). While the dimensionless kinetic heat flux $\langle w'\theta'\rangle(w_*\theta_*)^{-1}$ (11) decrease linearly with ζ (Figure 8), the dimensionless horizontal wind fluctuations are more or less constant

$$\frac{\sigma_u}{w_*} \approx \frac{\sigma_v}{w_*} \approx 0.6 \quad \text{(daytime CBL)}\,. \qquad (18)$$

To describe the behaviour of the dimensionless temperature and vertical wind standard deviation, empirical functions of ζ are established which exhibit a minimum of $\sigma_\theta\ \theta_*^{-1}$ and a maximum of $\sigma_w\ w_*^{-1}$ in the centre of the daytime CBL.

The daytime features of the statistical moments of second order could only partly be retrieved in the morning transition as observed by the Helipod. The dimensionless horizontal wind fluctuations did not show a systematic dependence on ζ (Figure 10). The mean values were found around

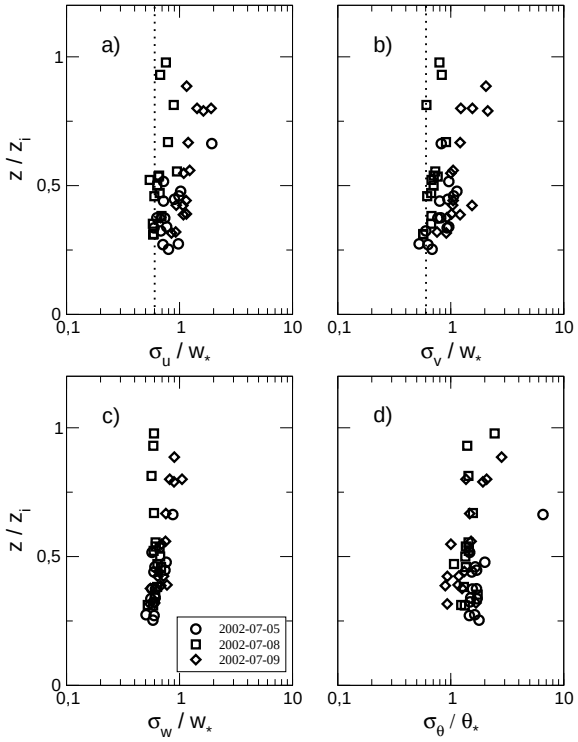

Fig. 10: Dimensionless standard deviations of a) wind along flight direction, b) cross wind, c) vertical wind, d) potential temperature.

$\sigma_u\ w_*^{-1} \approx \sigma_v\ w_*^{-1} \approx 0.9$ (Table 1) with some dependence on the day of measurement and increasing scatter with increasing ζ. Also in contrast to the daytime CBL both $\sigma_w\ w_*^{-1}$ (on average 0.65) and $\sigma_\theta\ \theta_*^{-1}$ (around 1.5) were found to be ζ-independent although again the scatter increased at larger ζ (and also an outlier occurred for $\sigma_\theta\ \theta_*^{-1}$ on 5 July). A substantial increase of scatter of the dimensionless statistical moments in the upper part of the daytime CBL was already observed in other experiments (Sorbjan 1991), possibly due to variations of the entrainment parameter A. Sorbjan (1996a) explained the scatter of moments involving the temperature with a variation of the potential lapse rate γ_i in the inversion. Hence Sorbjan (2005) recommended the use of an alternative set of adjusted similarity parameters containing γ_i. Since in our early-morning temperature profile (Figure 2) and in agreement with e.g., Deardorff (1967), Sorbjan (1996c) and Angevine *et al.* (2001), the lapse rate inside the inversion remained unchanged during the transition, the alternative parameters could not reduce the scatter in the data presented here.

4. CONCLUSIONS

On three days low-level flights during the morning transition were analysed in order to identify scales and parameters that simplify the characteristics of the SCBL. Many indications were found that the morning transitions were quasi-stationary and governed by linear processes. During the burn-off process the inversion lapse rate γ_i remained unchanged. The height of the inversion base, the surface temperature and the surface heat flux increased linearly in time. A quite good mixing of the SCBL was also expected due to the very short large eddy overturning time $\tau_* \leq 300$ s. Nevertheless, the development of the sensible heat flux $H(t)$ at the flight level was afflicted with larger deviations from linear behaviour. Consequently, scaling the flight level z with the inversion base z_i and the sensible heat flux H at z with the surface heat flux H_0 led to a vertical profile with large scatter, although the classic CBL heat flux profile could still be identified. A linear fit of the dimensionless heat flux started near the SCBL at about 0.8 z_i, crossed zero at 0.55 z_i and was extrapolated to the ground in good agreement with surface flux measurements.

Two reasons for the scatter in the dimensionless heat flux profile can be considered. In the SCBL the mean wind speed was low and the turbulent transport was dominated by vertical motion (up- and down-drafts due to convection). Nevertheless, the horizontal advection (as also discussed by Hibberd 1996; Sorbjan 1996c) and the horizontal turbulent fluxes – term S in (6) – had possibly a noticeable effect and could not be neglected. More likely, the scatter was due to the heterogeneous terrain of the STINHO-2 site. The atmospheric flow in the SCBL was significantly affect by the underlying surface (Lenschow *et al.* 1979) and the individual legs were flown over varying terrain. Overall the scatter in the dimensionless flux profile was not substantially larger than what is known from the daytime CBL (Sorbjan 1991). In fact the findings fit better into classic CBL theory than other observations during the morning transition (e.g. de Arellano *et al.* 2004).

Significant difference to the daytime CBL was found in the dimensionless standard deviations. The eddy overturning time τ_* was found to be

much smaller compared to the daytime CBL. As in the daytime CBL $\sigma_u\ w_*^{-1}$ and $\sigma_v\ w_*^{-1}$ were height-independent and more or less identical. But the mean values were found to be larger (0.9 instead of 0.6). Unlike in the daytime CBL the variances of vertical wind and temperature were height-independent ($\sigma_w\ w_*^{-1} \approx 0.65$ and $\sigma_\theta\ \theta_*^{-1} \approx 1.5$). In agreement with experimental observations in the daytime CBL the scatter of all statistical moments of second order increased with height. This was possibly due to entrainment variations but not due to fluctuations of the lapse rate γ_i.

In agreement with the daytime CBL a mean entrainment parameter $A \approx 0.3$ was found in the Deardorff flux scheme, although the data base close to the inversion was quite thin. The experimentally determined ratio $B = 0.55$ of flux zero-crossing and inversion height exceeded the estimated value of 0.4, which was derived from the linearised enthalpy equation. Possibly B was less time-independent than expected during the transition. But still B was found to be much smaller than in the daytime CBL, where the heat flux crosses zero usually around $0.8\ z_i$. If parameter B can be interpreted as a measure of the entrainment layer thickness, then the entrainment zone of the morning SCBL was much deeper than in the daytime CBL.

To enhance the data base on the morning transition additional flight experiments should be done. To reduce the amount of boundary parameters and sources of scatter, at first the SCBL over homogeneous terrain should be probed.

4. ACKNOWLEDGEMENTS

We are much obliged to Frank Beyrich and Jens-Peter Leps (MOL, DWD) who processed and provided the LAS, sodar and tower data. We like to thank Aline van den Kroonenberg and Zbigniew Sorbjan for discussion and advice. Special thanks to the crew of the FJS Helicopter Service in Damme (Germany) who performed the flights with the Helipod. The field experiment was funded by the German government (BMBF: EVA-GRIPS within DEKLIM, grant no. 01-LD-0301 and VERTIKO within AFO2000, grant no. 07-ATF-37).

REFERENCES

Angevine, W., **H. Baltink**, and **F. Bosveld**, **2001**: Observations of the Morning Transition of the Convective Boundary Layer. *Boundary-Layer Meteorol.*, **101**, 209 – 227.

de Arellano, J. V.-G., **B. Gioli**, **F. Miglietta**, **H. J. J. Jonker**, **H. K. Baltink**, **R. W. A. Hutjes**, and **A. A. M. Holtslag**, **2004**: Entrainment Process of Carbon Dioxide in the Atmospheric Boundary Layer. *J. Geophys. Res.*, **109**, doi:10.1029/2004JD004,725.

Bange, J., **F. Beyrich**, and **D. A. M. Engelbart**, **2002**: Airborne Measurements of Turbulent Fluxes during LITFASS-98: A Case Study about Method and Significance. *Theor. Appl. Climatol.*, **73**, 35–51.

Bange, J. and **R. Roth**, **1999**: Helicopter-Borne Flux Measurements in the Nocturnal Boundary Layer Over Land - a Case Study. *Boundary-Layer Meteorol.*, **92**, 295–325.

Bange, J., **P. Zittel**, **T. Spieß**, **J. Uhlenbrock**, and **F. Beyrich**, **2006**: A New Method for the Determination of Area-Averaged Turbulent Surface Fluxes from Low-Level Flights Using Inverse Models. *Boundary-Layer Meteorol.*, DOI: 10.1007/s10,546–005–9040–6.

Betts, A., **R. Desjardins**, **J. MacPherson**, and **R. Kelly**, **1990**: Boundary-Layer Heat and Moisture Budgets from FIFE. *Boundary-Layer Meteorol.*, **50**, 109–137.

Beyrich, F., **1997**: Mixing Height Estimation from Sodar - A Critical Discussion. *Atm. Environ.*, **21**, 3941–3953.

Beyrich, F., **F. Berger**, **H. de Bruin**, **T. Foken**, **W. Kohsiek**, **S. Richter**, and **U. Weisensee**, **2002**a: Experimental Determination of Turbulent Fluxes over the Heterogeneous LITFASS Area - Selected Results from the LITFASS-98 experiment. *Theor. Appl. Climatol.*, **73**, 19–34.

Beyrich, F., **H. A. R. de Bruin**, **W. M. L. Meijninger**, **J. W. Schipper**, and **H. Lohse**, **2002**b: Results from One-Year Continuous Operation of a Large Aperture Scintillometer over a Heterogeneous Land Surface. *Boundary-Layer Meteorol.*, **105**, 85–97.

Beyrich, F., **H.-J. Herzog**, and **J. Neisser**, **2002**c: The LITFASS Project of DWD and the LITFASS-98 Experiment: The Project Strategy and the

Experimental Setup. *Theor. Appl. Climatol.*, **73**, 3–18.

Deardorff, J. W., **1967**: Empirical Dependence of the Eddy Coefficient for Heat upon Stability Above the Lowest 50 m. *J. Appl. Meteorol.*, **6**, 631–643.

Deardorff, J. W., **1970**: Convective Velocity and Temperature Scales for the Unstable Planetary Boundary Layer and for Rayleigh Convection. *J. Atmos. Sci.*, **27**, 1211–1213.

Deardorff, J. W., **1974**: Three-Dimensional Numerical Study of the Height and Mean Structure of a Heated Planetary Boundary Layer. *Boundary-Layer Meteorol.*, **7**, 81–106.

Fedorovich, E., **R. Conzemius**, and **D. Mironov**, **2004**: Convective Entrainment into a Shear-Free, Linearly Stratified Atmosphere: Bulk Models Reevaluated through Large Eddy Simulations. *J. Atmos. Sci.*, **61**, 281–295.

Gossard, E. E., **J. E. Gaynor**, **R. J. Zamora**, and **W. D. Neff**, **1985**: Finestructure of Elevated Stable Layers Observed by Sounder and In Situ Tower Sensors. *J. Atmos. Sci.*, **42**, 2156–2169.

Hibberd, M. F., **1996**: Comments on 'Toward Evaluation of Heat Fluxes in the Convective Boundary Layer'. *J. Appl. Meteorol.*, **35**, 1370–1373.

Kaimal, J. C. and **J. J. Finnigan**, **1994**: *Atmospheric Boundary Layer Flows - Their Structure and Measurement*. Oxford University Press. 289 pp.

Kim, S.-W., **S.-U. Park**, and **C.-H. Moeng**, **2003**: Entrainment Processes in the Convective Boundary Layer with Varying Wind Shear. *Boundary-Layer Meteorol.*, **108**, 221–245.

Lenschow, D. H. and **B. B. Stankov**, **1986**: Length Scales in the Convective Boundary Layer. *J. Atmos. Sci.*, **43**, 1198–1209.

Lenschow, D. H., **B. B. Stankov**, and **L. Mahrt**, **1979**: The Rapid Morning Boundary-Layer Transition. *J. Atmos. Sci.*, **36**, 2108–2124.

Meijninger, W. M. L., **F. Beyrich**, **A. Lüdi**, **W. Kohsiek**, and **H. A. R. de Bruin**, **2005**: Area-Averaged Sensible and Latent Heat Fluxes using Large Aperture and Millimeter Wave Scintillometers. *Boundary-Layer Meteorol.*. Published online, DOI: 10.1007/s10546-005-9022-8.

Meijninger, W. M. L., **O. K. Hartogensis**, **W. Kohsiek**, **J. C. B. Hoedjes**, **R. M. Zuurbier**, and **H. A. R. de Bruin**, **2002**: Determination of Area-Averaged Sensible Heat Fluxes with a Large Aperture Scintillometer over a Heterogeneous Surface – Flevoland Field Experiment. *Boundary-Layer Meteorol.*, **105**, 37–62.

Muschinski, A. and **C. Wode**, **1998**: First In-Situ Evidence for Co-Existing Sub-Meter Temperature and Humidity Sheets in the Lower Free Troposphere. *J. Atmos. Sci.*, **55**, 2893–2906.

Neisser, J., **W. Adam**, **F. Beyrich**, **U. Leiterer**, and **H. Steinhagen**, **2002**: Atmospheric Boundary Layer Monitoring at the Meteorological Observatory Lindenberg as a Part of the 'Lindenberg Column': Facilities and Selected Results. *Meteorol. Z. N. F.*, **11**, 241–253.

Petre, J. M. and **J. Verlinde**, **2004**: Cloud Radar Observations of Kelvin-Helmholtz Instability in a Florida Anvil. *Mon. Wea. Rev.*, **132**, 2520–2523.

Raabe, A., **K. Arnold**, **A. Ziemann**, **F. Beyrich**, **J.-P. Leps**, **J. Bange**, **P. Zittel**, **T. Spieß**, **T. Foken**, **M. Göckede**, **M. Schröter**, and **S. Raasch**, **2005**: STINHO - Structure of Turbulent Transport under Inhomogeneous Surface Conditions – part 1: the Micro-α scale field experiment. *Meteorol. Z. N. F.*, **14**, 315–327.

Sorbjan, Z., **1991**: Evaluation of Local Similarity Functions in the Convective Boundary Layer. *J. Appl. Meteorol.*, **30**.

Sorbjan, Z., **1995**: Toward Evaluation of Heat Fluxes in the Convective Boundary Layer. *J. Appl. Meteorol.*, **34**, 1092–1098.

Sorbjan, Z., **1996**a: Effects Caused by Varying the Strength of the Capping Inversion based on a Large-Eddy Simulation Model of the Shear-Free Convective Boundary Layer. *J. Atmos. Sci.*, **53**, 2015–2024.

Sorbjan, Z., **1996**b: Numerical Study of Penetrative and 'Solid Lid' Nonpenetrative Convective Boundary Layers. *J. Atmos. Sci.*, **53**, 101–112.

Sorbjan, Z., **1996**c: Reply on Comments on 'Toward Evaluation of Heat Fluxes in the Convective Boundary Layer' by M. F. Hibberd. *J. Appl. Meteorol.*, **35**, 1374–1377.

Sorbjan, Z., **2005**: Statistics of Scalar Fields in the Atmospheric Boundary Layer based on

Large-Eddy Simulations. Part I: Free Convection. *Boundary-Layer Meteorol.*, **116**, 467–486.

Stull, R., **1988**: *Boundary Layer Meteorology*. Kluver Acad., Dordrecht, 666 pp. 666 pp.

Sullivan, P. P., **C.-H. Moeng**, **B. Stevens**, **D. H. Lenschow**, and **S. D. Mayor**, **1998**: Structure of the Entrainment Zone Capping the Convective Atmospheric Boundary Layer. *J. Atmos. Sci.*, **55**, 3042–3064.

Tennekes, H., **1973**: A Model for the Dynamics of the Inversion Above a Convective Boundary Layer. *J. Atmos. Sci.*, **30**, 558–567.

Tab. 1: Characteristics of the three flights during the morning transition.

		flight 1	flight 2	flight 3
date	2002	5 July	8 July	9 July
time	UTC	0520 – 0645	0557 – 0707	0539 – 0700
horizontal legs		13	16	15
vertical profiles		3	5	4
clouds		no clouds	no clouds	1/8 Ci
flight altitude z	m agl	82.6	90.0	85.1
RL base h	m agl	330	240	390
wind speed at 400 m	m s^{-1}	5.5	4.0	5.4
wind speed at z	m s^{-1}	2.9	2.9	4.9
$\dot{z}_i$	m h^{-1}	129	143	134
$\dot{\theta}(z)$	K h^{-1}	1.83	1.55	2.20
$\dot{H}(z)$	W m^{-2} h^{-1}	30.8	36.5	43.2
$\dot{H}_0$	W m^{-2} h^{-1}	58.4	54.8	66.6
B		0.37	0.47	0.42
$\sigma_u w_*^{-1}$		0.87 ± 0.33	0.69 ± 0.11	1.16 ± 0.30
$\sigma_v w_*^{-1}$		0.83 ± 0.18	0.71 ± 0.10	1.24 ± 0.40
$\sigma_w w_*^{-1}$		0.63 ± 0.10	0.60 ± 0.06	0.73 ± 0.13
$\sigma_\theta \theta_*^{-1}$		1.63 ± 0.15	1.53 ± 0.42	1.43 ± 0.52